Supplementary Information for:

Engineering heterointerface and composition for ultrathin broadband microwave absorbers based on high entropy oxides/alloys heterostructured composites

*Han Liu, Zhenyu Xu, Zhiyue He, Housheng Mao, Jiayang Lin, Naixin Zhai, Zhenzhi Cheng, Fei Gao, Guangsheng Luo, and Weiping Zhou**

School of Physics and Materials Science, Nanchang University, Nanchang 330031, People's Republic of China

* Authors to whom correspondence should be addressed: wpzhou@ncu.edu.cn.

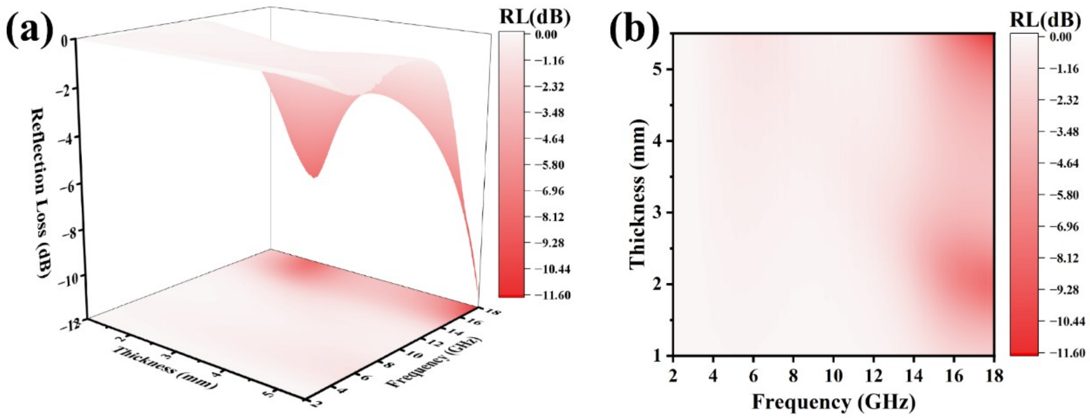

Fig. S1 Microwave absorption of the as-fabricated samples. The 3D plots of reflection loss (*RL*) (a) and the 2D *RL* contour plots (b) of $(Co_{0.2}Ni_{0.2}Cu_{0.2}Mn_{0.2}Mg_{0.2})Fe_2O_4$ at different thicknesses in the range of 2–18 GHz.

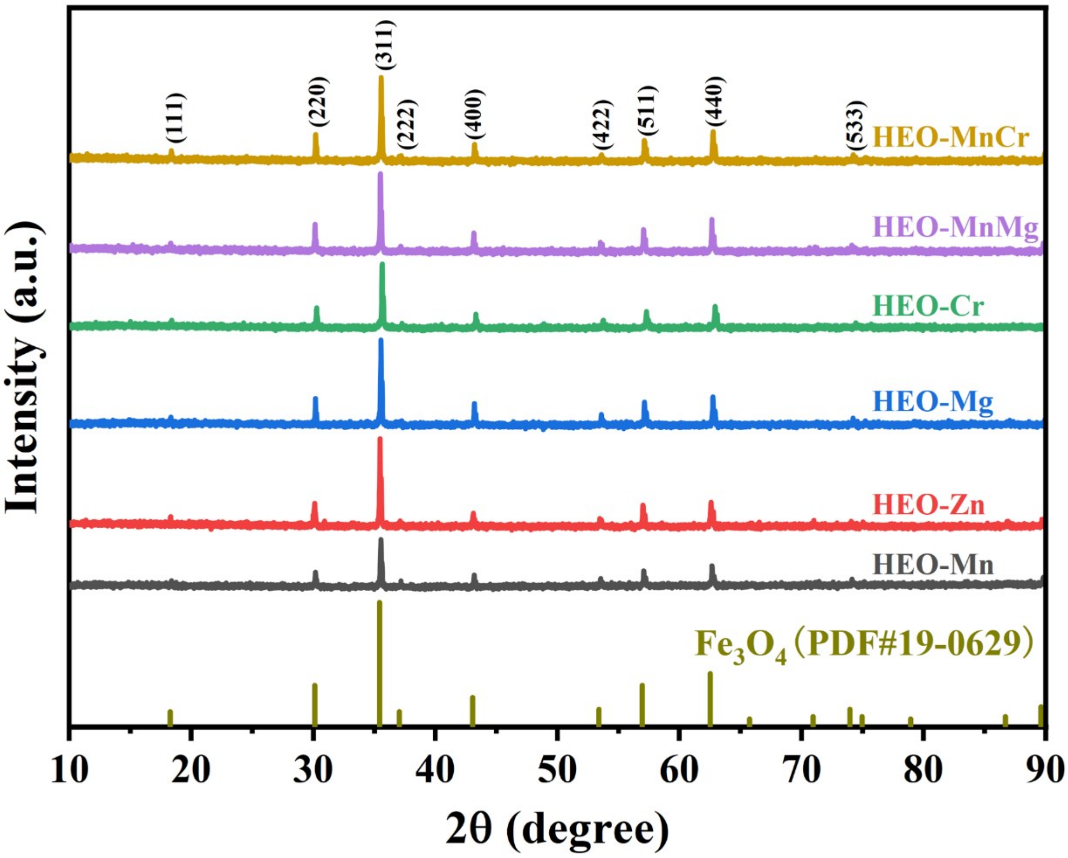

Fig. S2 The XRD patterns of six high entropy MFe_2O_4, HEO-Mn, HEO-Zn, HEO-Mg, HEO-Cr, HEO-MnMg, HEO-MnCr

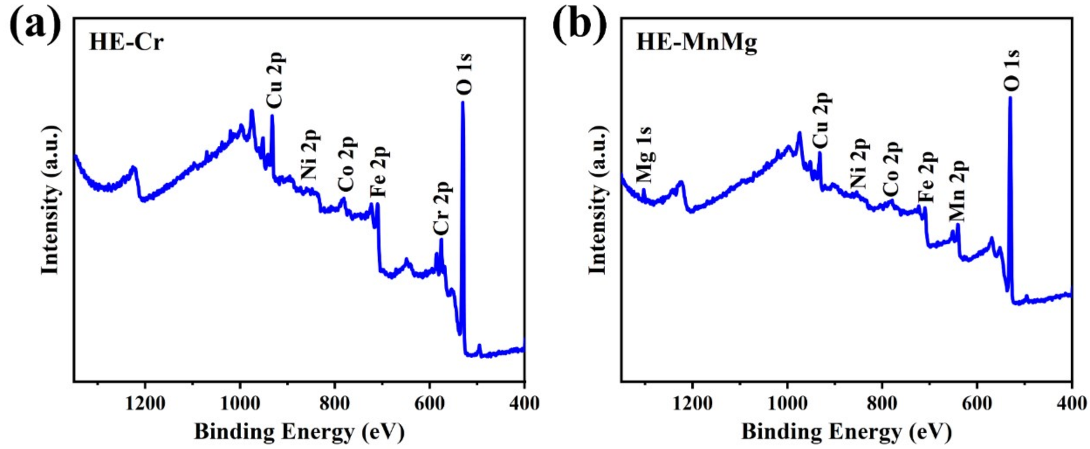

Fig. S3 XPS full spectra of (a) HE-Cr and (b) HE-MnMg.

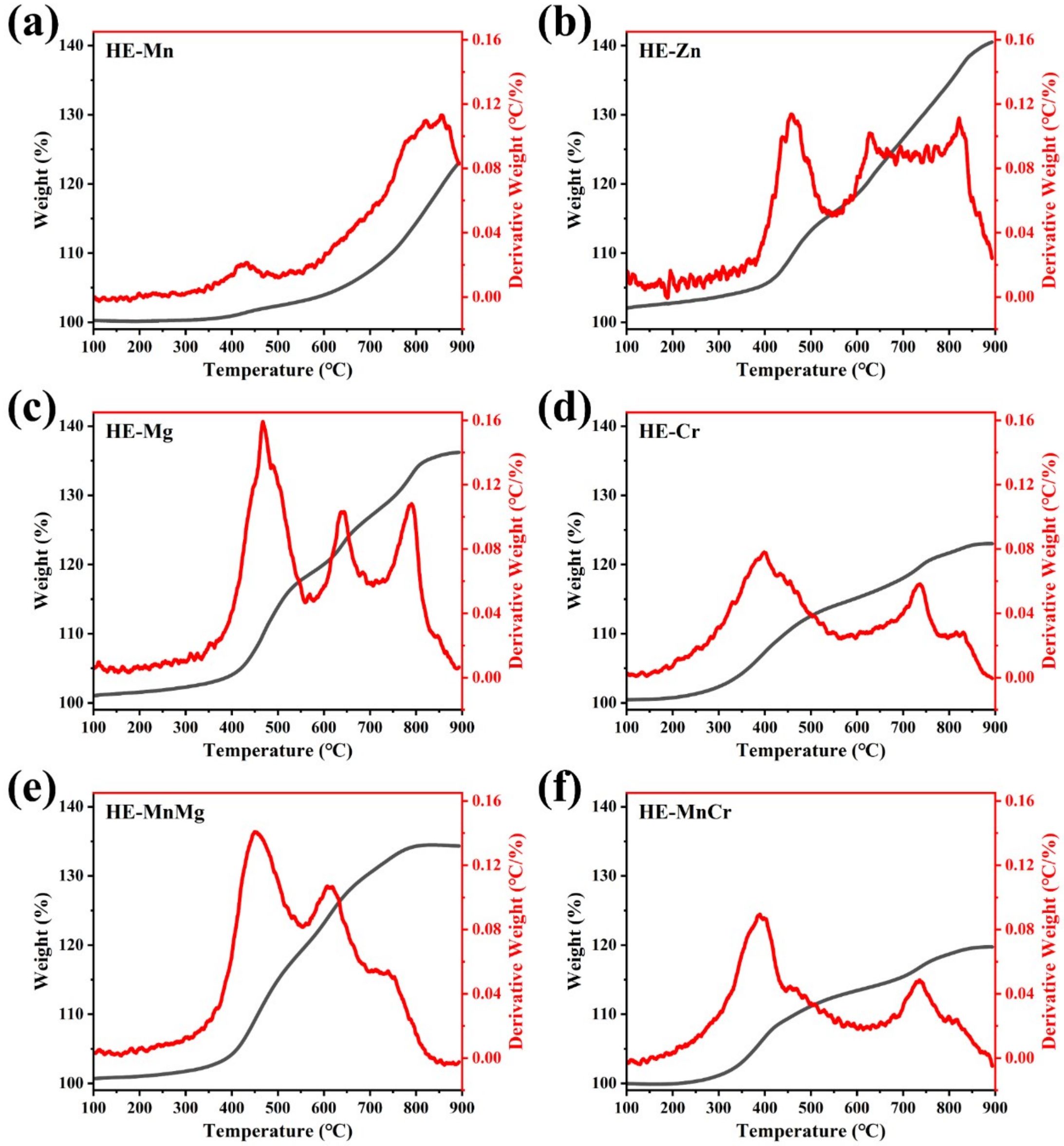

Fig. S4 TG curves and DTG (first-order derivatives of TG curves) of (a) HE-Mn, (b) HE-Zn, (c) HE-Mg, (d) HE-Cr, (e) HE-MnMg, (f) HE-MnCr.

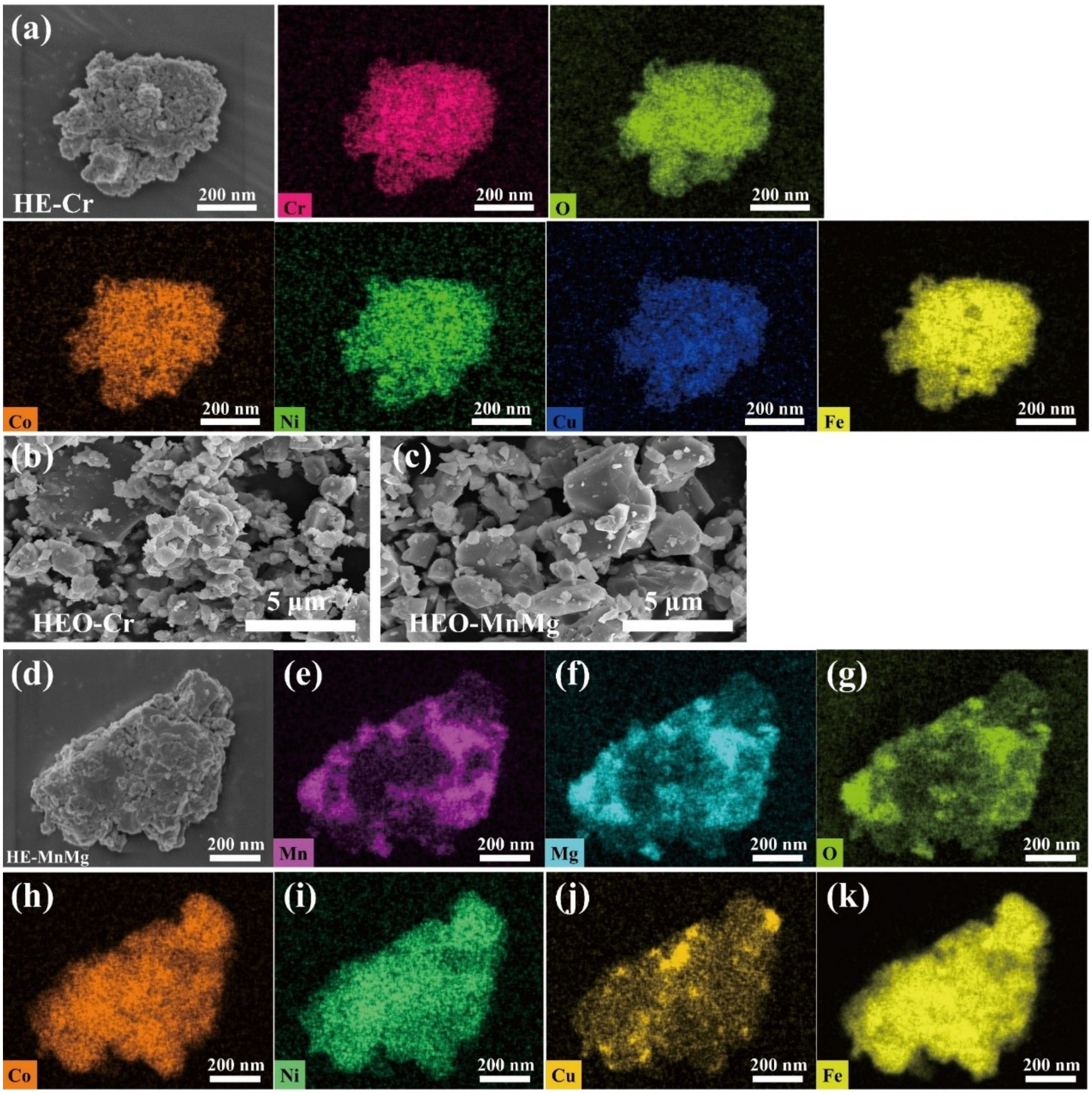

Fig. S5 (a) SEM images and EDS mapping of HE-Cr, SEM images of HEO ceramics, (b) HEO-Cr and (c) HEO-MnMg, (d) SEM image of HE-MnMg, (e-k) EDS mapping of each element in HE-MnMg.

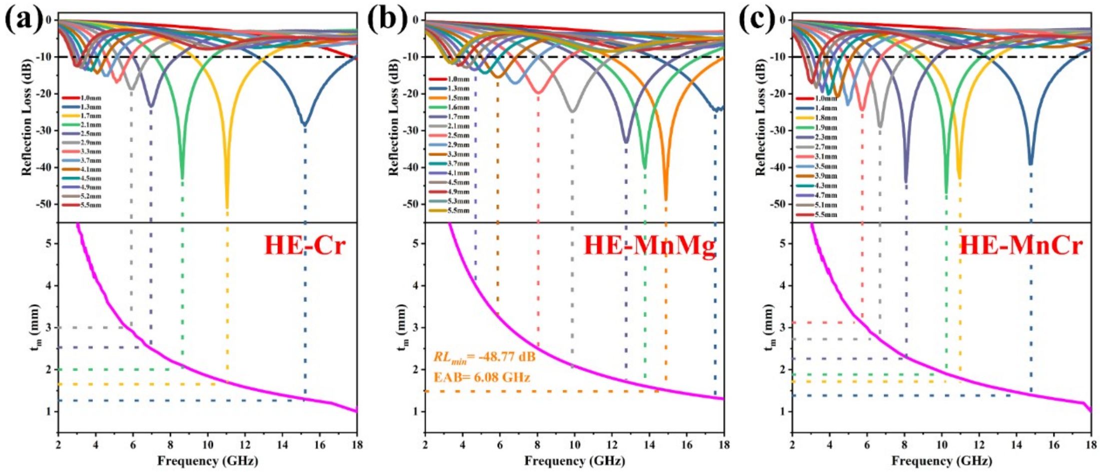

Fig. S6 The correspondence between the peak frequency of RL_{min} and the matching thickness under quarter-wave conditions, (a) HE-Cr, (b) HE-MnMg, (c) HE-MnCr.

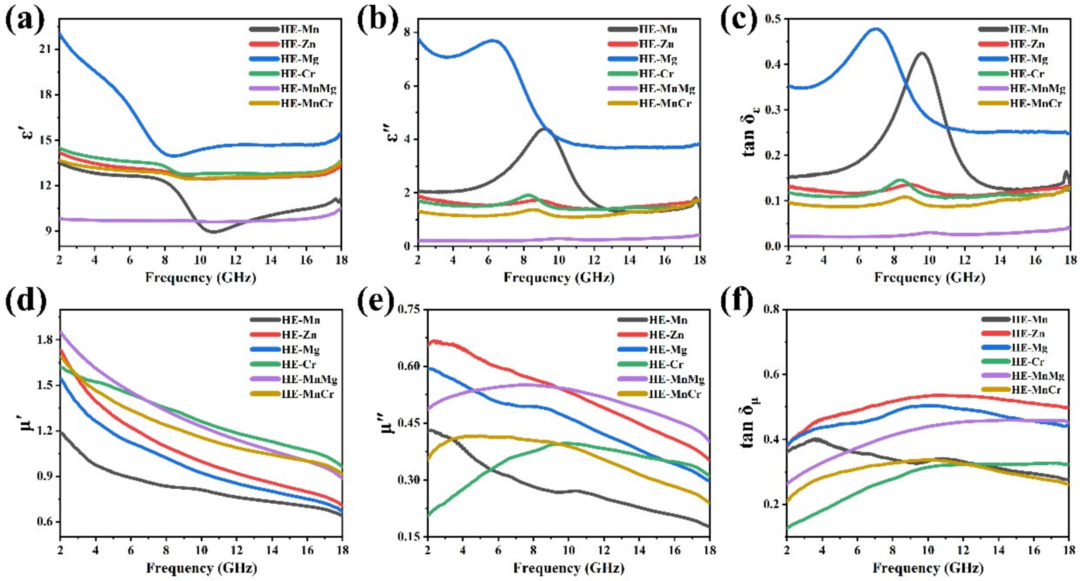

Fig. S7 (a) Real part and (b) imaginary part of permittivity, (c) the curves of tan δ_ε, (d) real part and (e) imaginary part of permeability, (f) the curves of tan δ_μ for HE-Mn, HE-Zn, HE-Mg, HE-Cr, HE-MnMg, HE-MnCr.

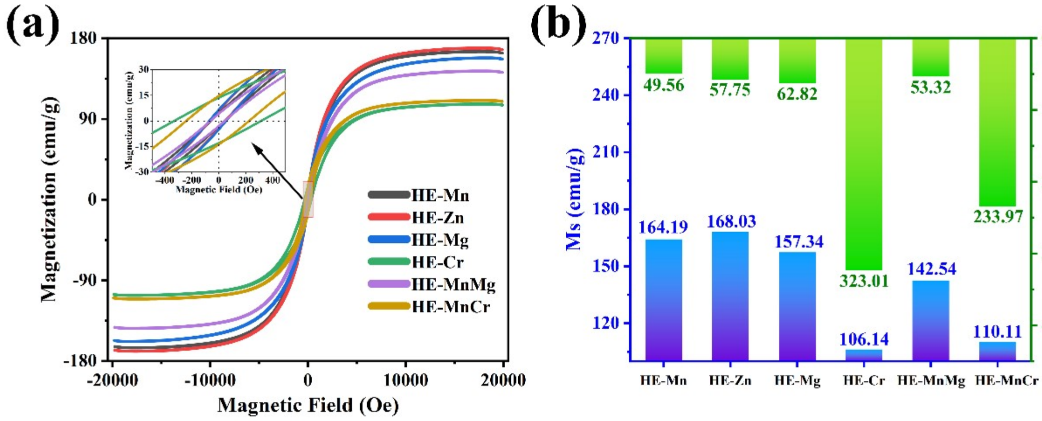

Fig. S8 (a) Hysteresis loops, (b) saturation magnetization (Ms) and coercivity (Hc) of HE-Mn, HE-Zn, HE-Mg, HE-Cr, HE-MnMg, HE-MnCr at room temperature.

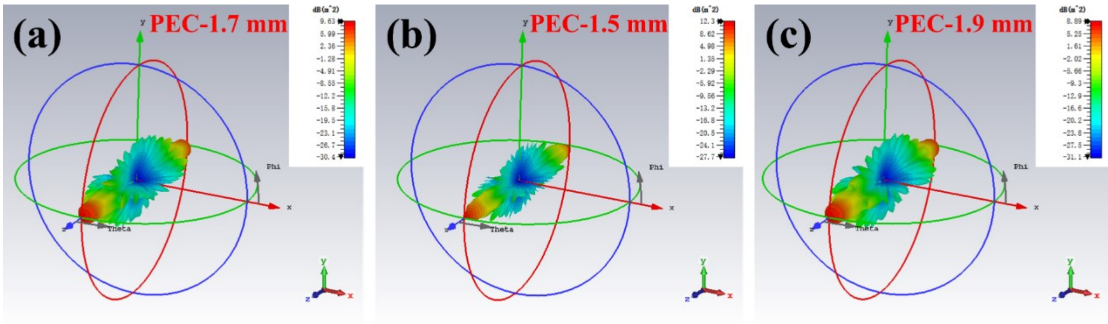

Fig. S9 The CST simulation results of PEC plate with thickness of (a) 1.7 mm, (b) 1.5 mm and (c) 1.9 mm.